CZECH TECHNICAL UNIVERSITY IN PRAGUE

FACULTY OF MECHANICAL ENGINEERING

DOCTORAL THESIS STATEMENT

Czech Technical University in Prague
Faculty of Mechanical Engineering
Department of Mechanics, Biomechanics and Mechatronics

DOCTORAL THESIS STATEMENT

PHENOMENOLOGICAL MODELING OF STRAIN-RANGE DEPENDENT CYCLIC HARDENING

Ing. Jaromír Fumfera

Doctoral Study Programme: Mechanical Engineering
Study Field: Mechanics of Rigid and Deformable Bodies and Environment

Supervisor: doc. Ing. Miroslav Španiel, CSc.

Doctoral statement for obtaining
the acamdemic title of "Doctor" abbreviated to "Ph.D."

Prague, September 2020

Thesis title: Phenomenological Modeling of Strain-Range Dependent Cyclic Hardening

This doctoral thesis is an outcome of a full-time form of doctoral study programme at the Department of Mechanics, Biomechanics and Mechatronics, Faculty of Mechanical Engineering, Czech Technical University in Prague.

Disertant: Ing. Jaromír Fumfera
Department of Mechanics, Biomechanics and Mechatronics
Faculty of Mechanical Engineering
Czech Technical University in Prague
Technická 4, 166 07 Prague 6, Czech Republic
Miro.Fumfera@gmail.com

Supervisor: doc. Ing. Miroslav Španiel, CSc.
Department of Mechanics, Biomechanics and Mechatronics
Faculty of Mechanical Engineering
Czech Technical University in Prague
Technická 4, 166 07 Prague 6, Czech Republic
Miroslav.Spaniel@fs.cvut.cz

Reviewers: _____

_____

_____

The thesis was sent on: .....

The thesis defense will take place on .....

The dissertation thesis is available at the Departement of Science and Research of Faculty of Mechanical Engineering, Czech Technical University in Prague, Technická 4, 166 07 Prague 6, Czech Republic.

.....
prof. Ing. Michael Valášek, DrSc.

Head of Doctoral Study Field Mechanics of Rigid and Deformable Bodies and Environment
Faculty of Mechanical Engineering, Czech Technical University in Prague

Title: Phenomenological Modeling of Strain-Range Dependent Cyclic Hardening

Abstract: This doctoral thesis deals with the phenomenological modeling of the material response of metals for large strain loading conditions. The main focus is on the phenomenon of material cyclic hardening and its dependency on the loading conditions, which was observed on the austenitic stainless steel 08Ch18N10T. The formulation of a metal plasticity constitutive model with a new cyclic hardening rule is proposed to enable correct simulation of the material response under large strain for uniaxial and torsional loading conditions. Material parameters of the presented model for 08Ch18N10T steel are identified. The constitutive model is implemented as a Fortran code in the commercial FE-software Abaqus as a material subroutine USDFLD. The extensive experimental program with 6 different specimen geometries made of 08Ch18N10T steel is presented. The results of FE simulations of all these cyclic tests are presented. A comparison of simulated and experimentally measured response shows the prediction capability of the presented material model.

Keywords: cyclic plasticity, extremly low-cycle fatigue, strain-range dependent, finite element analysis

Název: Fenomenologické modelování cyklického zpevnění materiálu závislého na hladině zatížení

Abstrakt: Tato práce řeší fenomenologické modelování odezvy kovových materiálů při velkých deformacích. Zaměřuje se především na jev cyklického zpevnění materiálu a jeho závislosti na podmínkách zatěžování, což bylo pozorováno např. u austenitické nerezové oceli 08Ch18N10T. Je formulován konstitutivní model cyklické plasticity s novou definicí cyklického zpevnění materiálu, která umožňuje korektně simulovat odezvu materiálu při velkých deformacích pro jenoosé i torzní namáhání. Pro popsaný model jsou určeny materiálové parametry pro ocel 08Ch18N10T. Je popsána implementace modelu do komerčního konečně-prvkového softwaru Abaqus pomocí uživatelské subrutiny USDFLD napsané v programovacím jazyce Fortran. Jsou prezentovány výsledky zkoušek rozsáhlého experimentálního programu provedeného na 6 různých geometriích zkušebních vzorků z oceli 08Ch18N10T. Na srovnání výsledků experimentů a jejich simulací jsou demonstrovány predičkní schopnosti navrženého modelu.

Klíčová slova: cyklická plasticita, extrémně nízko-cyklová únava, závislost na hladině deformace, metoda konečných prvků

Contents

1 Introduction

Low-cycle fatigue (LCF) is a part of the fatigue phenomenon, where loading implies higher nominal stresses than the yield strength. The maximum number of cycles to failure for common steel-like materials is usually less than thousands of cycles [1].

The prediction of LCF on real mechanical components consists of two key features - modeling of material response and choosing the appropriate criterion of failure. The appropriate criterion of failure predicts when a failure occurs in a mechanical component depending on loading conditions and its history. Loading conditions are stress and strain tensor fields.

In low-cycle fatigue, the yield strength is exceeded in a large volume of material, the plastic deformations occur and the relationship between stress and strain is no longer linear - on the contrary, it can be very complex.

Low-cycle fatigue, where only few dozens of cycles to failure is reached [2, 3] is usually called extremely-low-cycle fatigue (ELCF) [4, 2, 3] or according to some authors ultra-low-cycle fatigue [5] or very-low-cycle fatigue [6]. Between LCF and ELCF, there are some notable differences. Material models based on cyclically stable material, without correct reflection of cyclic hardening/softening, is unable to make an accurate prediction in the ELCF regime. This generates one more area currently being researched in conjunction with the LCF phenomenon, which is a material response for high-loading conditions, for example on the transition between LCF and ELCF regime.

For example, austenitic stainless steel 08Ch18N10T shows so called strain-range dependent cyclic hardening, as can be seen in Figure 1. For this material it means that it shows almost no cyclic hardening for low-loading conditions, a saturation of material response occurs under constant cyclic loading conditions and material is cyclically stable. But it shows continuous cyclic hardening with no saturation of material response under high-loading conditions. This phenomenon has to be somehow reflected in the material model if the fatigue prediction should give a satisfactory result.

2 State of the Art

2.1 Brief Introduction to the Theory of Plasticity

Plastic Strain

Total strain ϵ is defined as

$$\epsilon = \epsilon^e + \epsilon^p, \tag{1}$$

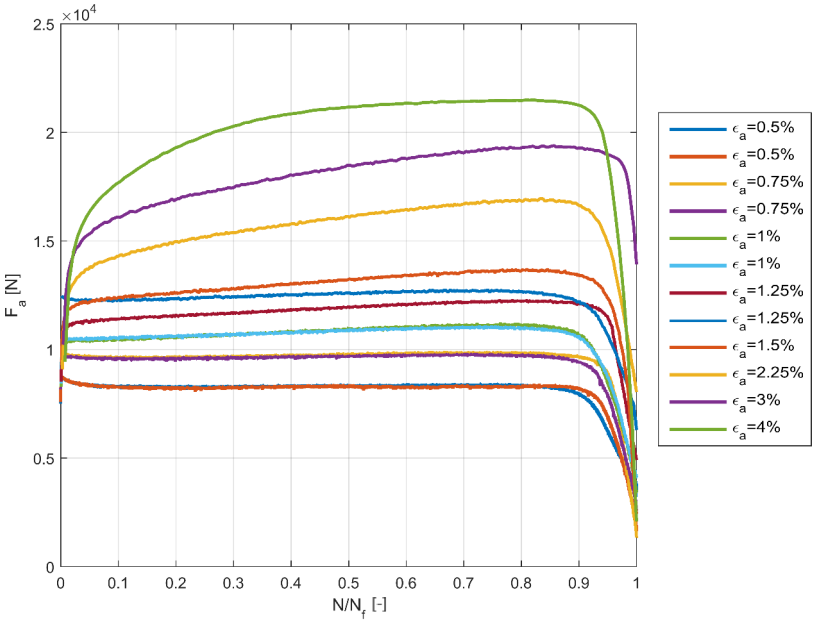

Figure 1: Illustration of strain-range dependent cyclic hardening of 08Ch18N10T stainless steel. [A5]

where ϵ^e is elastic strain and ϵ^p is plastic strain. Using Hooke's law, it can be formulated as

$$\sigma = E\epsilon^e = E(\epsilon - \epsilon^p), \tag{2}$$

where σ is stress and E is the Young modulus.

This simple uniaxial problem can be generalized for multiaxial loading conditions and can be expressed using tensor notation as

$$\boldsymbol{\sigma} = \boldsymbol{C}\boldsymbol{\epsilon}^{\boldsymbol{e}}, \tag{3}$$

where $\boldsymbol{\sigma}$ is elastic stress tensor, $\boldsymbol{\epsilon}^{\boldsymbol{e}}$ is elastic strain tensor and $\boldsymbol{C}$ is the elastic stiffness matrix.

For multiaxial loading, it is necessary to choose an appropriate criterion for determining the equivalent (sometimes also called effective) stress σ_e and for von Mises criterion it can be written as

$$\sigma_e = \frac{1}{\sqrt{2}}[(\sigma_1 - \sigma_2)^2 + (\sigma_2 - \sigma_3)^2 + (\sigma_3 - \sigma_1)^2]^{1/2}, \tag{4}$$

where $\sigma_{1,2,3}$ are principal stresses

An equivalent (sometimes also called effective) increment of plastic strain is defined as

$$dp = \left(\frac{2}{3} d\boldsymbol{\epsilon}^p : d\boldsymbol{\epsilon}^p\right)^{\frac{1}{2}} \simeq \left(\frac{2}{3} d\boldsymbol{\epsilon}' : d\boldsymbol{\epsilon}'\right)^{\frac{1}{2}}. \tag{5}$$

Condition of Plasticity and Normal Hypothesis

For von Mises yield criterion, the plasticity function is in general defined as

$$f = \sigma_e - Y = \left(\frac{3}{2}\boldsymbol{\sigma}' : \boldsymbol{\sigma}'\right)^{\frac{1}{2}}, \tag{6}$$

where Y is actual yield stress and $\boldsymbol{\sigma}'$ stands for deviatoric part of stress tensor. This function defines so-called yield surface, which for the von Mises criterion takes the form of a cylinder wall in the space of the principal stresses. The plasticity condition is then given as

$$f < 0 \text{ for elastic strain,} \tag{7}$$

$$f = 0 \text{ for plastic strain.} \tag{8}$$

For metal materials and von Mises plasticity is generally accepted that

$$d\boldsymbol{\epsilon}^p = \frac{3}{2} dp \frac{\boldsymbol{\sigma}'}{\sigma_e}. \tag{9}$$

The Consistency Condition

In the case of plastic loading, it is necessary to meet the so-called consistency condition, which can be interpreted so that the point representing the load must remain on the yield surface. This condition is given by the equation

$$f = \sigma_e - Y = 0 \tag{10}$$

and can be further customized.

Cyclic Stress-Strain Curve

If the common steel-like material is exposed to the uniaxial cyclic loading, the response of the material changes due to changes in microstructure. The intensity of these changes usually decreases with increasing number of cycles and after that, the response stabilizes [7]. The stabilized state can be illustrated by the hysteresis loop. The cyclic stress-strain curve (CSSC) is created by interposing the vertices of hysteresis loops for different ϵ_a.

Isotropic Hardening

The plasticity condition can be written as

$$f = \sigma_e - Y(p) = \sigma_e - (\sigma_y + R(p)), \tag{11}$$

where σ_y is yield strength and $R(p)$ is the isotropic variable. $R(p)$ can take various forms, for example, in commercial FE software Abaqus 6.14, the non-linear isotropic hardening model is defined as

$$R(p) = Q(1 - e^{-bp}), \tag{12}$$

where Q and b are material parameters [8].

Kinematic Hardening

The plasticity condition from the equation (6) then takes form

$$f = \sigma_e - Y = \left(\frac{3}{2}(\boldsymbol{\sigma}' - \boldsymbol{\alpha}') : (\boldsymbol{\sigma}' - \boldsymbol{\alpha}')\right)^{\frac{1}{2}} - Y = 0, \tag{13}$$

where $\boldsymbol{\alpha}$ is the so-called back-stress.

Chaboche [9] superpose the back-stress from m parts as

$$\boldsymbol{\alpha} = \sum_i^m \boldsymbol{\alpha}_i, \tag{14}$$

$$d\boldsymbol{\alpha}_i = \frac{2}{3} C_i d\boldsymbol{\epsilon}^p - \gamma_i \boldsymbol{\alpha} dp, \tag{15}$$

where m is usually equal to 2 or 3. Marquis [10] came with a modification using an evolutionary rule for the kinematic hardening for its non-linear term as

$$d\boldsymbol{\alpha} = \frac{2}{3} C d\boldsymbol{\epsilon}^p - \phi(p)\gamma_\infty \boldsymbol{\alpha} dp, \tag{16}$$

where ϕ is called Marquis parameter [7] or the ϕ function.

Combined Hardening Model

Combining the kinematic and isotropic hardening model, the plasticity condition then has the form

$$f = \left(\frac{3}{2}(\boldsymbol{\sigma}' - \boldsymbol{\alpha}') : (\boldsymbol{\sigma}' - \boldsymbol{\alpha}')\right)^{\frac{1}{2}} - \sigma_y + R(p). \tag{17}$$

Strain-Range Dependent Cyclic Hardening

Adjusting the plasticity equations (16) and (17), taking into account the load level and using the memory surface concept, the plasticity function can be written as:

$$f = \left(\frac{3}{2}\left(\boldsymbol{\sigma}' - \boldsymbol{\alpha}'(p, R_M)\right) : \left(\boldsymbol{\sigma}' - \boldsymbol{\alpha}'(p, R_M)\right)\right)^{\frac{1}{2}} - \sigma_y + R(p, R_M), \quad (18)$$

$$d\boldsymbol{\alpha} = \frac{2}{3} C d\boldsymbol{\epsilon}^p - \phi(p, R_M) \cdot \gamma_\infty \boldsymbol{\alpha} dp, \quad (19)$$

where R_M is the size of the memory surface.

2.2 Some Important Publications Related to Strain-Range Dependent Cyclic Plasticity

Most of this chapter is directly cited from the article [A1].

"Phenomenological models [11] are the most widely-used models in practical applications. Their goal is to provide as accurate as possible description of the stress-strain behavior of the material, which is found on the basis of experiments [12]. The stress-strain behavior of structural materials under cyclic loading is very diverse, and a case-by-case approach is required [13].

The most progressive group of cyclic plasticity models, which are commonly encountered in commercial finite element method programs, are single yield surface models based on differential equations. Their development is closely linked to the creation of a nonlinear kinematic hardening rule with a memory term, introduced by Armstrong and Frederick in 1966 for the evolution of back-stress [14], and the discovery by Chaboche [9] of the vast possibilities offered by the superposition of several back-stress parts.

Developments in the field of non-linear kinematic hardening rules were mapped in detail in [11]. In the current paper, we will mention only the most important theories. In 1993, Ohno and Wang [15] proposed two nonlinear kinematic hardening rules. For both models, it is considered that each part of the back-stress has a certain critical state of dynamic recovery. Ohno-Wang Model I leads to plastic shakedown under uniaxial loading with a nonzero mean axial stress value (no ratcheting), and under multiaxial loading it gives lower accumulated plastic strain values than have been observed in experiments. The memory term of Ohno-Wang Model II [15] is partially active before reaching the critical state of dynamic recovery, which allows a good prediction of ratcheting under uniaxial loading and also under multiaxial loading. The Abdel-Karim-Ohno nonlinear kinematic hardening rule [16] was published in 2000. This rule is in fact a superposition of the Ohno-Wang I and

Armstrong-Frederick rules. The proposed model was designed to predict the behavior of materials that exhibit a constant increment of plastic strain during ratcheting. Other modifications to this kinematic hardening rule, leading to a better prediction of uniaxial ratcheting and also multiaxial ratcheting, were proposed by one of the authors of paper [17]. In order to capture the additional effects of cyclic plasticity, the concept of kinematic and isotropic hardening has been further modified. Basically, the available theories can be divided into two approaches. The first approach is related to the actual distortion of the yield surface [18, 19, 20], while the second approach is related to the memory effect of the material [9], [21]. The effect of cyclic hardening as a function of the size of the strain amplitude is usually assumed in the second approach.

The first comprehensive model of cyclic plasticity with a memory surface was proposed by Chaboche and co-authors in [9]. Chaboche's memory surface was established in the principal plastic strain space and captures the influence of plastic strain amplitude and also the mean value of the plastic strain. The memory surface is associated with a non-hardening strain region in a material point, as is explained by Ohno [21] for the general case of variable amplitude loading. Memory surfaces established in the stress space have also been developed. Their main advantage is that they enable more accurate ratcheting strain prediction to be achieved, as presented by Jiang and Sehitoglu in their robust cyclic plasticity model [22]. Good agreement with experiments has been achieved in the case of steel SS304 [23], but at the cost of defining more than 70 material parameters.

Of recently published works, Halama et al [A1] developed a new cyclic plasticity model suitable for predicting strain-range dependent cyclic hardening of austenitic steels. The model is capable of capturing the cyclic hardening with strain-range dependency as for example Kang advanced model [23], but with a considerably lower number of material parameters, as has been demonstrated in [A1].

2.3 Material Parameters Identification

E, ν and σ_y are usually determined from the tensile test according to [24] or other equivalent standard. Material parameters of the Chaboche model C_i and γ_i can be determined from the cyclic stress-strain curve or from the large hysteresis loop [25].

For strain-range dependent hardening materials, material parameters fitted from large hysteresis loop usually does not predict well the shape of smaller hysteresis loops. This is usually corrected by determining the Marquis parameter ϕ and isotropic variable R as a function of accumulated plastic strain p and memory surface R_M [A1].

3 Motivation

In the framework of the grant project of Czech Technological Agency TA04020806, on which the author participates, extensive experimental research program of the LCF of austenitic stainless steel 08Ch18N10T has been done. The most advanced suitable model, that can predict strain-range dependent cyclic hardening of this material, while still holding back the number of material parameters, turns out to model of cyclic plasticity developed by Halama et al [A1]. In this thesis, it will continue to be referred to as the original model.

The model shows excellent prediction capability for uniaxial loading conditions. It also predicts well the response of notched specimens on three different notched geometries.

Under torsional loading conditions, the original model does predict the material response well only for lower loading levels. However, the original model (as, of course, it's predecessors) over-predicts cyclic hardening of 08Ch18N10T steel for higher loading levels. In order to minimize the observed over-prediction under torsional loading conditions, a new formulation of material model is needed.

4 Objectives of the Doctoral Thesis

The main objective of the thesis is to propose a new formulation of a constitutive model that can predict the response of the material for uniaxial loading conditions as well as for the torsional loading conditions. The key steps to achieve this goal are:

1. **The proposition of modification:**

   Modifications of the original model will be proposed and new constitutive relations will be described.

2. **Calibration of material parameters:**

   The material parameters of the newly proposed model will be identified for 08Ch18N10T austenitic stainless steel. The identification process will be described step by step, the new set of material parameters for 08Ch18N10T steel will be presented.

3. **Implementation into FE:**

   Building FE models of specimens, that have been used for experiments (presented in Chapter 3) will be described. The newly proposed model will be implemented into commercial FE software Abaqus as a user subroutine USDFLD. The algorithm of the subroutine as well as the full Fortran code of the subroutine will be presented.

5 Experimental Program

The experimental program mentioned in section 3 has been focused on LCF of austenitic stainless steel 08Ch18N10T. The material parameters identification series (IDF) was therefore compiled from uniform-gage (UG) specimens (see Figure 2) and non-uniform-gage specimens with an elliptical longitudinal section (E9), see Figure 3). The next series consists of E9 geometry, notch geometry with an $R = 1.2\,\text{mm}$ (R1.2, see Figure 4), geometry with an $R = 2.5\,\text{mm}$ notch (R2.5, see Figure 5) and geometry with an $R = 5\,\text{mm}$ notch (R5, see Figure 6). The last series is the notched tube geometry (NT, see Figure 7) which was exposed to torsional loading.

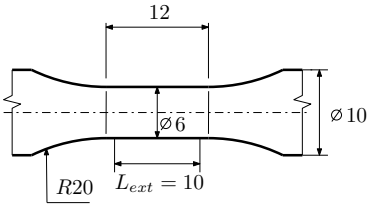

Figure 2: Sketch of UG geometry. [A2]

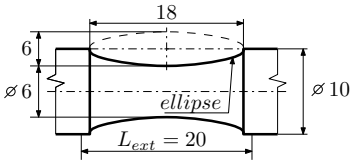

Figure 3: Sketch of E9 geometry. [A2]

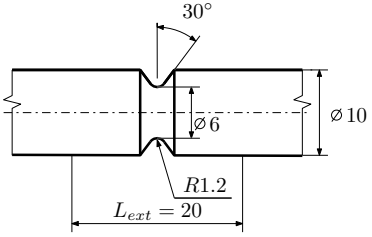

Figure 4: Sketch of R1.2 geometry. [A2]

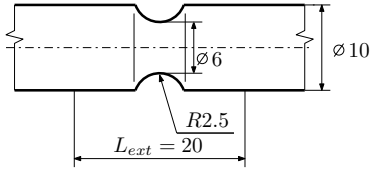

Figure 5: Sketch of R2.5 geometry. [A2]

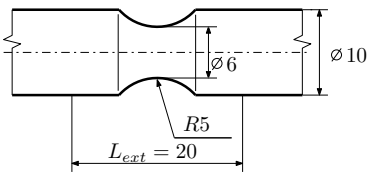

Figure 6: Sketch of R5 geometry. [A2]

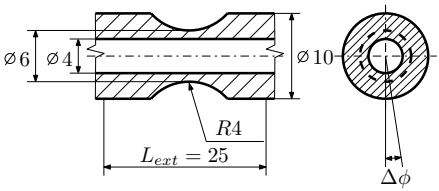

Figure 7: Sketch of NT geometry. [A2]

6 Constitutive Model of Cyclic Plasticity

6.1 The Original Model

Yield Surface and Flow Rule

The single yield surface concept for the metallic materials, based on the von Mises yield criterion, is used. The plasticity function is defined as

$$f = \sqrt{\frac{2}{3}(\boldsymbol{\sigma'} - \boldsymbol{\alpha'}) : (\boldsymbol{\sigma'} - \boldsymbol{\alpha'})} - Y = 0, \tag{20}$$

where $\boldsymbol{\sigma'}$ is the deviatoric part of the stress tensor $\boldsymbol{\sigma}$, $\boldsymbol{\alpha'}$ is the deviatoric part of the back-stress $\boldsymbol{\alpha}$ and Y is the actual yield stress. The actual yield stress Y is defined as

$$Y = \sigma_Y + R, \tag{21}$$

where R is the isotropic variable and σ_y is the yield strength.

"The associative plasticity is considered, so the normality flow rule is considered in the case of active loading

$$d\boldsymbol{\epsilon}^p = d\lambda \frac{\partial f}{\partial \boldsymbol{\sigma}}. \tag{22}$$

Accumulated plastic strain increment dp is defined as

$$dp = \sqrt{\frac{2}{3} d\boldsymbol{\epsilon}^p : d\boldsymbol{\epsilon}^p}." \text{ [A1]} \tag{23}$$

The accumulated plastic strain is generally defined as

$$p = \int dp \tag{24}$$

Virtual Back-Stress

"A new internal variable is established to provide an easy way to calibrate the model. The variable is the back-stress of a cyclically stable material corresponding to the response of the material investigated under a large strain range. It will be referred to as the virtual back-stress. The Chaboche superposition of the back stress parts is used in the following form

$$\boldsymbol{\alpha}_{virt} = \sum_{i=1}^{M} \boldsymbol{\alpha}_{virt}^{i} \tag{25}$$

taking into consideration the nonlinear kinematic hardening rule of Armstrong and Frederick [14] for each part

$$d\boldsymbol{\alpha}_{virt}^{i} = \frac{2}{3} C_i d\boldsymbol{\epsilon}_p - \gamma_i \boldsymbol{\alpha}_{virt}^{i} dp, \tag{26}$$

where C_i and γ_i are material parameters. For all calculations in this paper the superposition of three kinematic hardening rules ($M = 3$) will be used." [A1]

Memory Surface

"A scalar function is introduced to represent the memory surface in the deviatoric stress space

$$g = \|\boldsymbol{\alpha}_{virt}\| - R_M \leq 0, \tag{27}$$

where R_M is the size of the memory surface and $\|\boldsymbol{\alpha}_{virt}\|$ is the magnitude of the total virtual back-stress. The evolution equation ensuring the possibility of memory surface expansionis therefore

$$dR_M = H(g) \left\langle \boldsymbol{L} : d\boldsymbol{\alpha}_{virt} \right\rangle, \tag{28}$$

where

$$\boldsymbol{L} = \frac{\boldsymbol{\alpha}_{virt}}{\|\boldsymbol{\alpha}_{virt}\|}." \text{ [A1]} \tag{29}$$

Kinematic Hardening Rule

"Consistent with the previous sections, the back-stress is composed of M parts

$$\boldsymbol{\alpha} = \sum_{i=1}^{M} \boldsymbol{\alpha}_i, \tag{30}$$

but the memory term is dependent on the size of memory surface R_M and accumulated plastic strain p, thus

$$d\boldsymbol{\alpha}_i = \frac{2}{3} C_i d\boldsymbol{\epsilon}_p - \gamma_i \phi(p, R_M) \boldsymbol{\alpha}_i dp, \tag{31}$$

where C_i and γ_i are the same as in equation (26). The multiplier ϕ of parameters γ_i is composed of a static part and a cyclic part

$$\phi(p, R_M) = \phi_0 + \phi_{cyc}(p, R_M), \tag{32}$$

where ϕ_0 has the meaning of a material parameter, while the cyclic part is variable and can change only in the case of $\dot{R}_M = 0$. In this case, the evolution equation is defined in the following way

$$d\phi_{cyc} = \omega(R_M) \cdot (\phi_\infty + \phi_{cyc}(p, R_M))\, dp. \tag{33}$$

$$\phi_\infty(R_M) = A_\infty R_M^4 + B_\infty R_M^3 + C_\infty R_M^2 + D_\infty R_M + F_\infty, \tag{34}$$

$$\omega(R_M) = A_\omega + B_\omega R_M^{-C_\omega} \text{ for } R_M \geq R_{M\omega}, \tag{35}$$

$$\omega(R_M) = A_\omega + B_\omega R_{M\omega}^{-C_\omega} \text{ otherwise}, \tag{36}$$

where A_∞, B_∞, C_∞, D_∞, F_∞, A_ω, B_ω, C_ω, $R_{M\omega}$ and R_{M0} are additional parameters to Chaboche's material parameters C_i and γ_i." [A1]

Isotropic Hardening Rule

"Continuous cyclic hardening has been observed for austenitic stainless steels for a large strain range under uniaxial loading [23]. To capture this behavior, we introduce the linear isotropic hardening rule

$$dR = R_0(R_M) dp, \tag{37}$$

where parameter R_0 is dependent on the size of the memory surface

$$R_0(R_M) = A_R R_M^2 + B_R R_M + C_R \text{ for } R_M \geq R_{M0}, \tag{38}$$

$$R_0(R_M) = A_R R_{M0}^2 + B_R R_{M0} + C_R \text{ otherwise}, \tag{39}$$

because of the strong dependence on the strain range observed in the experiments [23]." [A1]

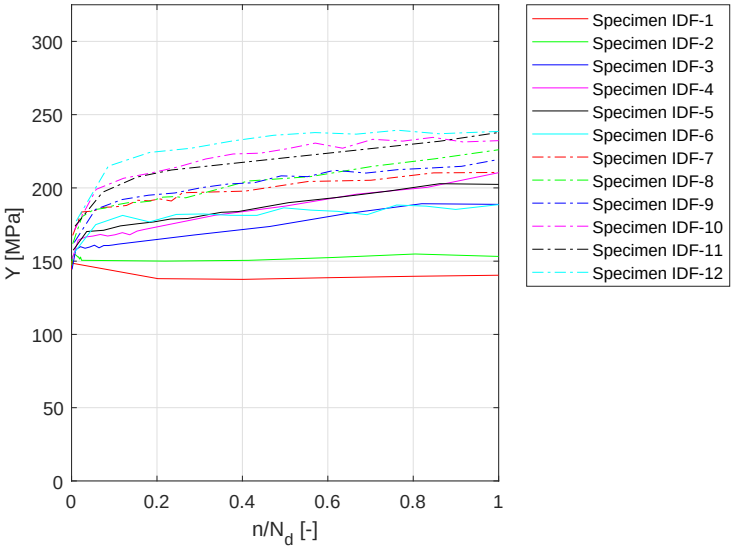

Figure 8: The evolution of actual yield stress Y during fatigue life for IDF specimen series.

6.2 Analysis of the Original Model

Isotropic hardening, as is defined in the original model by equation (37), is linear function of accumulated plastic strain p. But as can be seen in Figure 8, it does not reflect how the Y evolves during the fatigue life in 08Ch08N10T steel. This finding offers scope for a new definition of isotropic hardening that better reflects the actual yield stress development during the fatigue life.

The modification must also be strain-range dependent and the only possible way is through the modification of the memory surface definition for shear loading.

6.3 Modification for Shear Stress

New Formulation of Memory Surface

As the most effective way to deal with the problem of shear loading conditions, the author choose to define two memory surfaces - the first one to control the isotropic hardening, the second one to control the kinematic hardening. This concept was published in [A2].

The definition of the memory surface for the kinematic hardening $R_{M\phi}$ is newly modified. Using one extra material parameter, K_{shear}, the evolution

equations are modified to capture the torsional loading conditions as well as the uniaxial ones.

"The new memory surface $R_{M\phi}$ for the kinematic hardening part is modified and is defined by analogy as

$$\boldsymbol{\alpha}_{virt\phi} = \sum_{i=1}^{M} \boldsymbol{\alpha}^i_{virt\phi} \tag{40}$$

$$d\boldsymbol{\alpha}^i_{virt\phi} = \frac{2}{3} C_i d\boldsymbol{\epsilon}_p - \gamma_i K \boldsymbol{\alpha}^i_{virt\phi} dp \tag{41}$$

where

$$K = (\delta_{IJ} + (1 - \delta_{IJ}) K_{shear}) \tag{42}$$

where δ_{IJ} is Kronecker delta, I, J are indexes of stress tensor $\boldsymbol{\sigma}$ and K_{shear} is a new material parameter." [A2]

"The rest of the equations for defining the memory surface of the kinematic hardening part remain analogous to the original model [A1].

"The second modification to the original model [A1], also associated with the memory surface, is to omit limits $R_{M\omega}$ and R_{M0} and to set boundaries of the memory surfaces instead: R_M^{min} and R_M^{max}. The value of the memory surface R_M and $R_{M\phi}$ used for controlling the isotropic and kinematic hardening part can lie only between these two bounds. For simplification, and for mathematically correct expression, the memory surface size that is used, R_M^{used}, is defined as

$$R_M^{used} = R_M^{min} \text{ for } R_M < R_M^{min} \tag{43}$$

$$R_M^{used} = R_M \text{ for } R_M^{min} < R_M < R_M^{max} \tag{44}$$

$$R_M^{used} = R_M^{max} \text{ for } R_M > R_M^{max} \tag{45}$$

and analogously for $R_{M\phi}^{used}$." [A2]

Kinematic Hardening

The kinematic hardening equations is now defined as

$$d\boldsymbol{\alpha}_i = \frac{2}{3} C_i d\boldsymbol{\epsilon}_p - \gamma_i \phi(p, R^{used}_{M\phi}) \boldsymbol{\alpha}_i dp \tag{46}$$

$$\phi(p, R^{used}_{M\phi}) = \phi_0 + \phi_{cyc}(p, R^{used}_{M\phi}) \tag{47}$$

$$d\phi_{cyc} = \omega(R^{used}_{M\phi}) \cdot \left(\phi_\infty + \phi_{cyc}(p, R^{used}_{M\phi})\right) dp \tag{48}$$

$$\phi_\infty(R^{used}_{M\phi}) = A_\infty(R^{used}_{M\phi})^4 + B_\infty(R^{used}_{M\phi})^3 + C_\infty(R^{used}_{M\phi})^2 + D_\infty R^{used}_{M\phi} + E_\infty \tag{49}$$

$$\omega(R^{used}_{M\phi}) = A_\omega + B_\omega(R^{used}_{M\phi})^{-C_\omega}. \tag{50}$$

This modification has been published in [A2].

New Formulation of Isotropic Haredning

For higher levels of loading, the actual yield stress Y is a non-linear function of N. For periodic loading with approximately constant amplitude, $N \approx p$, so Y also must be a non-linear function of p. For this reason, the isotropic hardening is newly defined as a non-linear function in p (instead of a linear definition in the original model [A1]) as

$$dR = A_R \cdot \exp(B_R \cdot R^{used}_M) \cdot p^{C_R}, \tag{51}$$

where A_R, B_R and C_R are material parameters. This modification has been published in [A2].

7 Material Parameters Identification

The material parameters of the proposed material model have been identified for the original experimental data of austenitic stainless steel 08Ch18N10T using the Matlab software.

Due to complexity of the strain-range dependent cyclic hardening of this material, the author decided to modify the existing approaches and to develop the new calibration method. This method is based on direct simulation of the material response using the incremental material model of cyclic plasticity in the same way as is used in FEA simulations. No analytical simplification has been used, all the material parameters have been identified using multiple optimizations process to match the hysteresis loop shape or amplitude between experiment and simulation.

7.1 Chaboche Material Parameters

The material parameters for uniaxial loading has been identified using 12 specimens, marked by the abbreviation IDF in the following text, each specimen representing a different level of loading. “According to the ASTM standard [26], the classic uniform-gage geometry of the specimen is limited up to the

amplitude of the total strain $\epsilon_a = 0.5\,\%$. For higher strain levels, an hourglass type geometry is required. According to this standard, the IDF specimens were compiled from uniform-gage geometry (specimens IDF1-IDF5) and hourglass geometry (specimens IDF6-IDF12)." [A1].

The design of the hourglass geometry has been found in order to prevent buckling during the testing. The process of finding the optimal design of the hourglass geometry is described in detail in [A5] and [A11].

Following text is directly cited from [A1]. "The loading force F applied to the IDF specimen was known, as was the strain field of the surface of the specimen. The strain field was measured by the extensometer in the case of uniform-gage geometry, or by the digital image correlation method in the case of hourglass geometry. Considering the uniaxial stress field in the cross section of a specimen, the stress can be determined as $\sigma = \frac{F}{A}$, where A is the cross section surface of the specimen. This allows the use of a different calibration process, based on knowledge of the shape of the stress-strain hysteresis loops in all cycles during the experiment to failure.

Let us select one hysteresis stress-strain loop of a point on the specimen representing one loading cycle. This can be optimally simulated by a set of material parameters C_1, γ_1, C_2, γ_2, C_3, γ_3 and σ_y. However, in the next cycle, the optimal set of these parameters can be slightly different, as can the set of parameters of a specimen with different loading conditions. This material model uses the memory surface concept by setting these material parameters as functions of R_M and making these coefficients dependent on the loading history and the loading level conditions.

The material model did not include a simulation of the material damage process, so only experimental data up to damage were used for the calibration. The number of cycles used is N_d, and this number corresponded with the drop in the loading force during the experiment by $2\,\%$, due to crack initiation and propagation leading to failure.

First, the fatigue life is divided into about 10 evenly spaced parts by selecting hysteresis loops (SHLs), and the cycle number of each selected hysteresis loop (SHL) is given as $N \simeq N_d/k$, where $k = 1, 2, \ldots, 10$. The Young modulus E, the Poisson ratio ν and the yield strength σ_y were determined from tensile test according to ISO standard [24].

σ_y can be interpreted as the point where the linear part of the static stress-strain curve turns into the non-linear part. The root mean squared error method ($RMSE$) can be applied to find the point. In the tensile test (or in the first cycle of the cyclic test), the yield strength σ_y corresponded to $RMSE \approx 8$. Applying $RMSE = 8$ to each SHL, the actual yield stress Y was found.

Two SHLs were chosen, the bigger one and the smaller one, each with cycle number $N = N_d$ (the last cycle). The Chaboche material model parameters

C_1, γ_1, C_2, γ_2, C_3, γ_3 were found using an optimization process. The target function is set to the optimal shape match between simulation and experiment of the two SHLs." [A1] The basic algorithm of Chaboche parameters identification process has been taken from [A12]. The results of calibration process for optimal Chaboche parameters are shown in Figure 9.

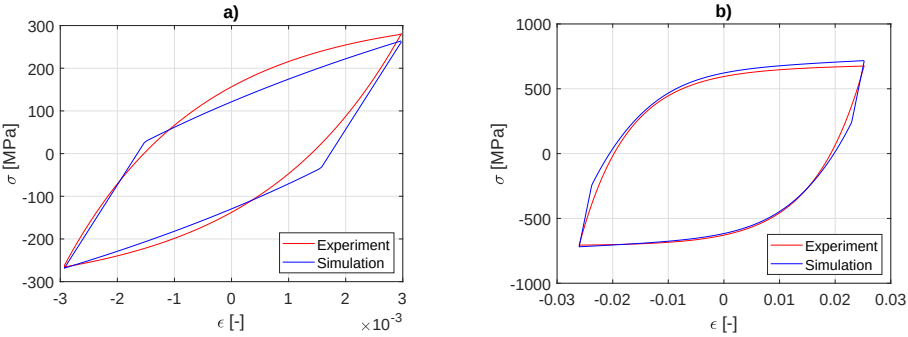

Figure 9: Chaboche material parameters fitting: (**a**) small hysteresis loop, (**b**) large hysteresis loop. [A1]

7.2 Cyclic Hardening Parameters

"Knowing the Chaboche material parameters, a first guess of the memory surface size for each specimen was determined. The formulation of R_M and the constant amplitude of the loading conditions resulted in fast saturation of the R_M value for each specimen (after the first cycle), which makes the calibration process easier." [A1]

"It is assumed here that $R_{M\phi} \simeq R_M$. Boundary parameters R_M^{min} and R_M^{max} are simply the maximum and minimum values of R_M computed in the identification process." [A2] Due to the experimental setup and the method of controlling the cyclic test, ϵ_a is almost, but not completely constant during the whole fatigue life for hourglass specimens, so the mean value of ϵ_a has been calculated. Details of determining the mean value can be found in [A8].

"The yield stress is now fitted as a function of R_M, using equation (51), by finding the material parameters A_R, B_R and C_R." [A1]

"Using the static stress-strain curve experimental data and performing a simulation of this curve, parameter ϕ_0 was found using equation (46) as an optimal value of ϕ for the static stress-strain curve simulation."[A1] The error between experimental static stress-strain curve and the simulation is calculated discretely using the least square method.

"The value of function ϕ from equation (46) was found for SHLs, using a similar optimization process as for determining the Chaboche material

parameters."[A1] This step defines the ideal value of the Marquis parameter ϕ for each SHL. "ϕ_∞ was the value of ϕ for $N = N_d$ and, from equation (49), ϕ_∞ was then set as a function of R_M by finding the material parameters A_∞, B_∞, C_∞,D_∞ and F_∞. The function ω determined the transition of the function ϕ between its border values ϕ_0 and ϕ_∞. Knowing the course of function ϕ during the fatigue life, ω was determined as a function of R_M by finding the material parameters A_ω, B_ω and C_ω from equation (50). This result was not necessarily optimal, so one more optimization was performed to find better ϕ_∞ and ω material parameters. The target function was set to the best possible match of the amplitude stress response between simulation and experiment during the whole fatigue life (not only SHLs)."[A1] Simulation results after the final process of material parameter identification is compared with the experimental data on Figure 10.

"The R_M value for each specimen was determined only as a first guess, so a number of iterations of the whole calibration process had to be carried out to find the final and optimal set of material parameters." [A1] The complete code of the material model is used for this optimization (here only converted from Fortran to Matlab programming language).

7.3 Torsional Loading

"For each NT geometry specimen tested, the $Error$ value in each cycle between the experimental amplitude of torque T_a^{exp} and the simulation amplitude of torque T_a^{sim} can be defined as

$$Error = (T_a^{exp} - T_a^{sim})/T_a^{exp} \cdot 100\,[\%]. \tag{52}$$

The $MeanError$ over all cycles is calculated as

$$MeanError = \frac{1}{N_d} \sum_{N=1}^{N_d} Error_n, \tag{53}$$

where index N is the number of cycles. The total error over all NT geometry specimens tested is defined as

$$TotalError = \frac{1}{S} \sum_{s=1}^{S} MeanError_s \tag{54}$$

where s is the NT specimen index and $S = 8$ is the total number of NT specimens tested " [A2]

"For the different K_{shear} from equation (42), the $TotalError$ value is captured in Figure 11. The final K_{shear} material parameter is identified as the optimal value of K_{shear} where the $TotalError$ is minimal. The material value parameters are presented in Table 1." [A2]

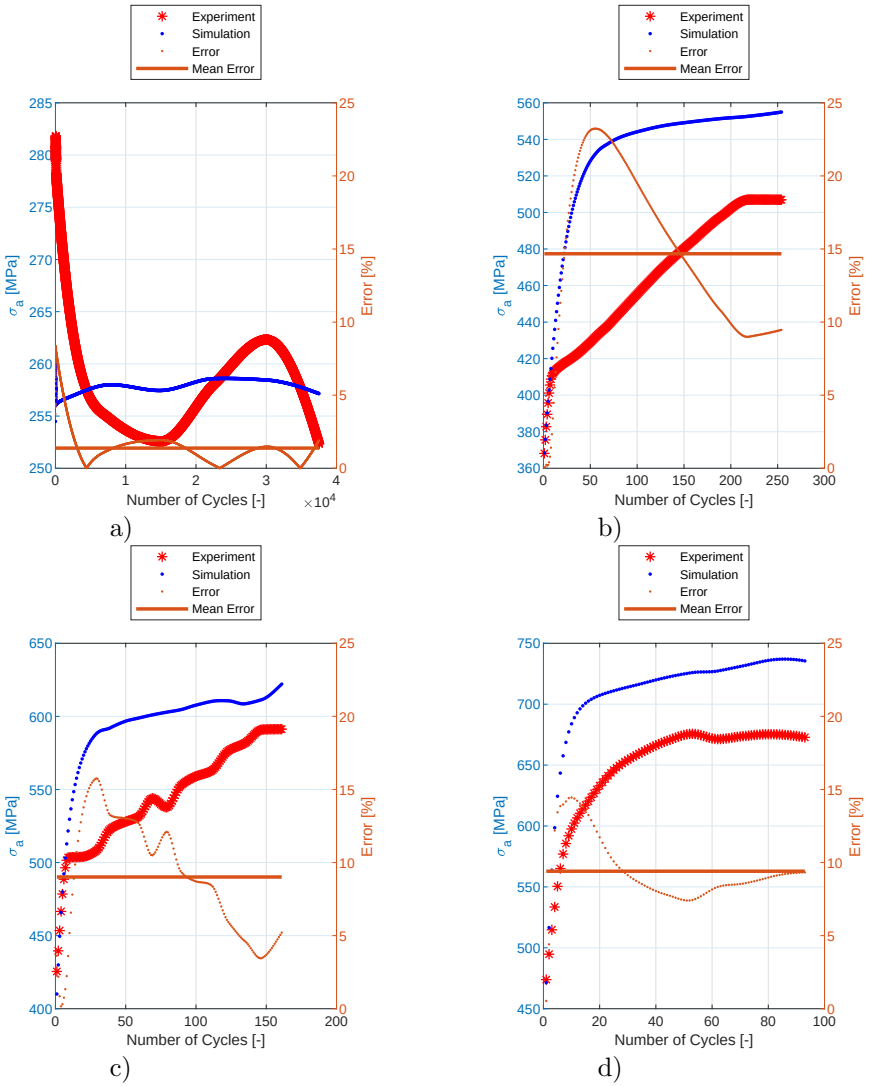

Figure 10: Experiment vs. simulations for selected IDF specimens: (**a**) specimen IDF1, (**b**) specimen IDF5, (**c**) specimen IDF9, (**d**) specimen IDF12.

8 Implementation of Proposed Model into Finite Element Analysis

"The geometry of most specimens is not uniform, so the non-uniform stress and strain field in their cross-section are expected and FEA must be used for

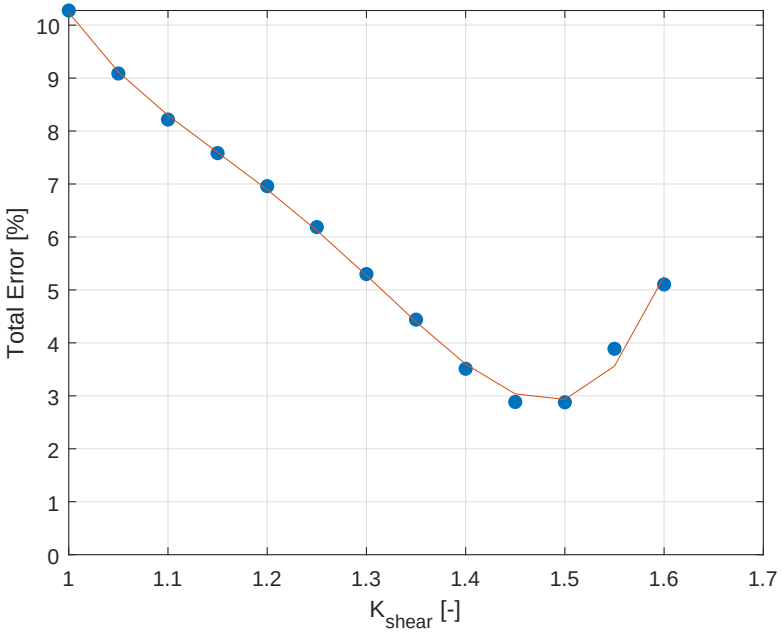

Figure 11: Identification of the K_{shear} material parameter. [A2]

Table 1: Material parameters of the new proposed model for 08Ch18N10T. [A2]

$\boldsymbol{E}$ [MPa]	$\boldsymbol{\nu}$	$\boldsymbol{\sigma_y}$ [MPa]	$\boldsymbol{C_1}$ [MPa]	$\boldsymbol{\gamma_1}$
210,000	0.3	150	63,400	148.6
$\boldsymbol{C_2}$ [MPa]	$\boldsymbol{\gamma_2}$	$\boldsymbol{C_3}$ [MPa]	$\boldsymbol{\gamma_3}$	$\boldsymbol{A_\infty}$
10,000	911.4	2000	0	-1.3127×10^{-9}
$\boldsymbol{B_\infty}$	$\boldsymbol{C_\infty}$	$\boldsymbol{D_\infty}$	$\boldsymbol{F_\infty}$	$\boldsymbol{A_R}$ [MPa^{-1}]
1.7981×10^{-6}	-8.6705×10^{-4}	1.6678×10^{-1}	-10.600	3.0113×10^{-1}
$\boldsymbol{B_R}$	$\boldsymbol{C_R}$ [MPa]	$\boldsymbol{R_M^{min}}$ [MPa]	$\boldsymbol{A_\omega}$	$\boldsymbol{B_\omega}$
1.4865×10^{-1}	1.1818×10^{-2}	130.54	0	2.0024×10^{-13}
$\boldsymbol{C_\omega}$	$\boldsymbol{R_M^{max}}$ [MPa]	$\boldsymbol{\phi_0}$	$\boldsymbol{K_{shear}}$	
-4.8591	506.59	2.3178	1.5	

simulations." [A2]. The constitutive model is implemented into Abaqus FE software using the USDFLD subroutine. The example of practical use can be found in [A6], where the proposed material model is used to simulate the pipe flange load. The displacement boundary condition respects amplitude value

as was recorded from the extensometer during the experiment.

8.1 FE Model

FE models of each of the tested geometries were created. The UG, E9, and notched geometries R1.2, R2.5, and R5 are modeled as an axisymmetric model, the NT geometry is modeled as a 3D model using cyclic symmetry.

8.2 Implementation of Material Model Using USDFLD Subroutine

The result of the USDFLD subroutine code for the proposed material model is the definition of $FIELD(1) = Y$ and $FIELD(2) = \phi$. The brief logic of building the USDFLD subroutine can be summerized in following points:

- Variables and material parameters are defined.
- Vector of plastic strain $\boldsymbol{\epsilon^p}$ and accumulated plastic strain p are obtained from previous increment.
- Flow vector is calculated.
- Vectors $\boldsymbol{\alpha_{virt}}$ and $\boldsymbol{\alpha_{virt\phi}}$ are calculated.
- The equations leading to determining the size of memory surfaces R_M^{used} and $R_{M\phi}^{used}$ are calculated.
- The isotropic variable R is calculated, actual yield stress is determined as $Y = \sigma_y + R$.
- Variables ϕ_∞, ω and ϕ_{cyc} are calculated.
- Variable ϕ is calculated.
- Some variables are stored to user defined state variable output $STATEV$ (for control purposes only).
- $FIELD$ array values for current increment are defined as $FIELD(1) = Y$, $FIELD(2) = \phi$.

9 Main Results

The error between the experiment and the FE simulation in each cycle N is calculated simply as

$$Error = \frac{F_a^{exp} - F_a^{sim}}{F_a^{exp}} \cdot 100\,\%. \tag{55}$$

The mean error and the total error are calculated using equations (53) and (54) considering the corresponding number of specimens in the series.

The Figures 12 and 13 show the experimental and simulation results of E9 geometry series representing the uniaxial loading conditions. The prediction capability of these two models is comparable. Results have been published in [A1] and [A2].

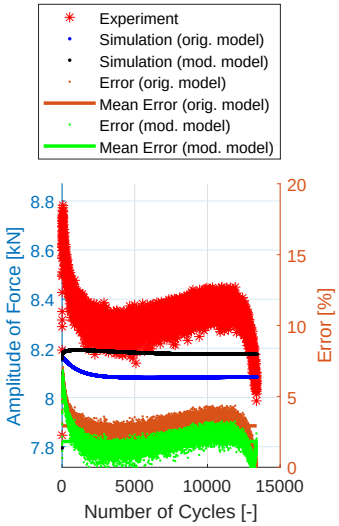

Figure 12: Experiment vs. simulations, specimen E9-1. [A1], [A2]

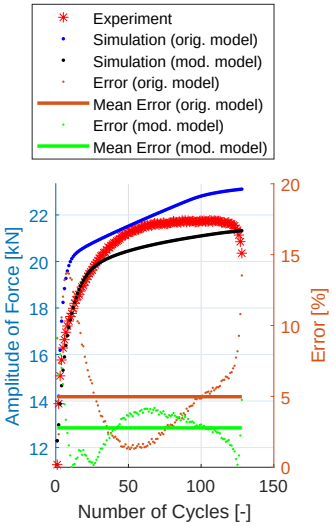

Figure 13: Experiment vs. simulations, specimen E9-17. [A1], [A2]

The NT geometry series results are shown in Figures 14 and 15. In this case, the compared variables are the amplitudes of the torque measured during the experiment ($T_{a\ exp}$) and the amplitudes computed by the FE simulations ($T_{a\ sim}$). The errors are calculated using the equations (52-54). For this geometry, the difference in the prediction capability of the original model and the modified model is not the same - the modified model provides a better prediction of the cyclic hardening of the material under torsional loading for higher loading levels. The results have been published in [A2].

Finally, the notched specimen geometry series R1.2, R2.5, and R5 are shown in Figures 16, 17, 18, 19, 20, and 21. The stress field in the cross-section of these specimens is no longer uniaxial, for more details see [A10], where the simulations of stress field in notched specimens has been presented. The prediction capabilities of both models are also comparable, the results have been published in [A2].

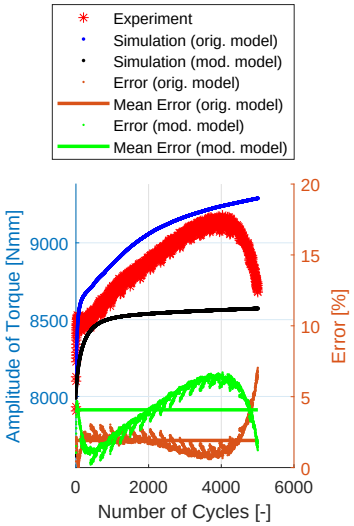

Figure 14: Experiment vs. simulations, specimen NT-1. [A2]

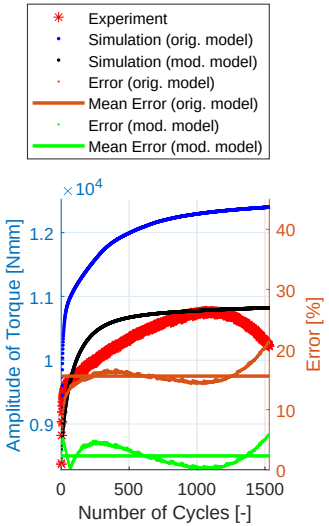

Figure 15: Experiment vs. simulations, specimen NT-6. [A2]

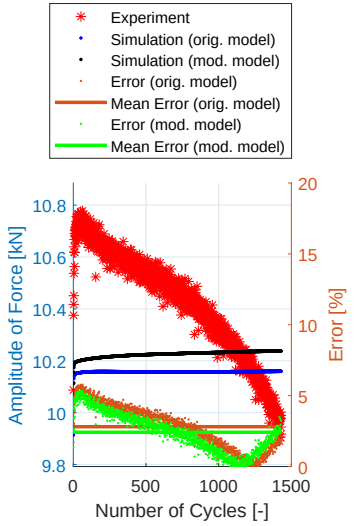

Figure 16: Experiment vs. simulations, specimen R1.2-1. [A2]

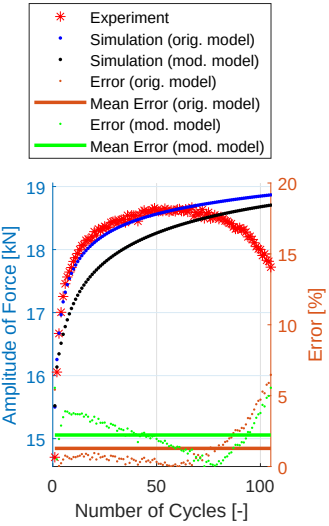

Figure 17: Experiment vs. simulations, specimen R1.2-18. [A2]

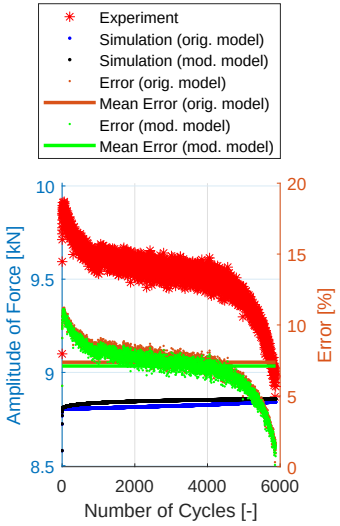

Figure 18: Experiment vs. simulations, specimen R2.5-1. [A2]

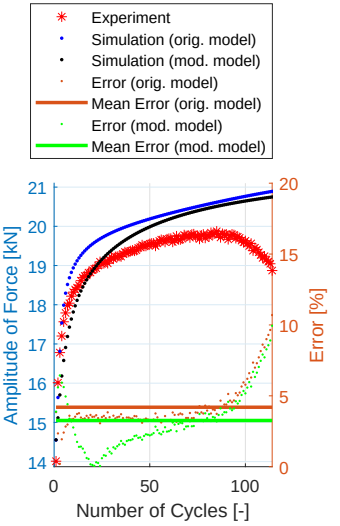

Figure 19: Experiment vs. simulations, specimen R2.5-21. [A2]

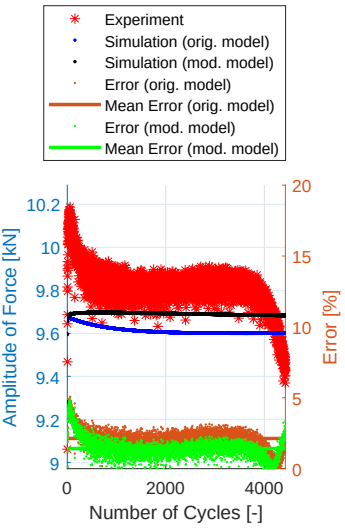

Figure 20: Experiment vs. simulations, specimen R5-1. [A2]

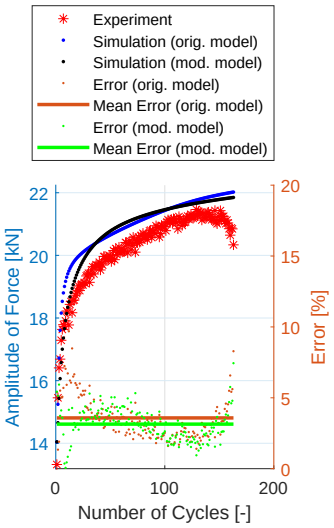

Figure 21: Experiment vs. simulations, specimen R5-24. [A2]

10 Outcomes

10.1 Theoretical Outcomes

The new material model, proposed in Section 6.3, is capable of capturing strain-range dependent hardening for uniaxial and newly also for torsional loading conditions. The proposed modification shows one of the possible ways to deal with the anisotropy between tension and torsion of the memory surface-based models.

The proposed material identification process, presented in Chapter 7, shows the new, unorthodox way to identify material parameters using the incremental FEA-like simulations of material response and multiple optimization procedure to fit the material parameters as precisely as possible. The identification process is also published in [A1], [A2], [A3] and [A7].

The implementation of the proposed model (presented in Chapter 8) is in the form of the Abaqus FE software user-defined field (USDFLD) subroutine. This will eventually allow other researchers to effectively modify or extend the proposed model and speed up the development of functional FE code.

10.2 Practical Outcomes

The new material model presented in the thesis is implemented into the commercial FE software Abaqus as the USDFLD subroutine. The implementation is described in Chapter 8 and also published in [A1] and [A2]. This allows potential users to test the proposed material model for real engineering computations, as has been demonstrated for example in [A6].

The material parameters identification process is described step by step in Chapter 7 and also published in [A1], [A2], [A4] and [A9]. Using the procedure, material parameters can be identified for other materials. The values of material parameters for 08Ch18N10T austenitic stainless steel are presented in Table 1.

Combination of presented USDFLD subroutine with material parameters for 08Ch18N10T steel, the newly proposed material model is ready for testing for engineering computations on real components.

11 Conclusion and Future Work

11.1 Conclusion

In this thesis, the original material model of cyclic plasticity with strain-range dependency published in [A1] is presented in Section 6. The constitutive equations are analyzed, the isotropic hardening part of the model and the

definition of memory surface are chosen as parts of the original model to be modified.

The fulfillment of the main objectives of the thesis, defined in Chapter 4, is summed up here:

1. **Proposition of modification:** The new formulation of the material model is proposed in section 6.3 and is also published in [A2]. The new formulation of isotropic hardening as a non-linear function of accumulated plastic strain p is proposed. The original memory surface is newly split into two memory surfaces - the memory surface for isotropic hardening, which is defined in the same way as the original one, and the memory surface for kinematic hardening, which is defined by the new constitutive equations. The new memory surface limits are defined.

2. **Calibration of material parameters:** The new calibration procedure of material parameters is proposed in this thesis. It uses the incremental FEA-like simulations of material response for fitting material parameters and multiple optimization procedure to fit the material parameters as precisely as possible. The material parameters identification process of newly proposed model is described step by step in Chapter 7 and is also published in [A1], [A2], [A3] and [A7]. Material parameters are identified for 08Ch18N10T austenitic stainless steel.

3. **Implementation into FE:** The implementation of the newly proposed model into FE code is described in 8 and also published in [A2]. The implementation into commercial FE software Abaqus is in the form of the user-defined field subroutine (USDFLD) written in Fortran programming language.

The newly proposed model shows practically the same prediction capability as the original for uniaxial and notched specimens, but significantly better prediction capability under torsional loading.

11.2 Future Work

The presented material model extends the good prediction capabilities of the original model [A1] from uniaxial to torsional loading. The dominant tensile or torsional loading is also the limitation of model usability in the proposed form. The next logical step is to verify the proposed model for combined loading conditions, for example, a proportional combination of tension and torsion and possibly propose another modification to include these loading conditions.

References

[1] Lemaitre, J. and Desmorat, R. *Engineering Damage Mechanics*. Springer (2005). ISBN 3-540-21503-4.

[2] Liu, R., Zhang, Z. J., Zhang, P., and Zhang, Z. F. Extremely-low-cycle fatigue behaviors of Cu and Cu–Al alloys: Damage mechanisms and life prediction. *Acta Materialia*, 83:341–356 (2015). doi: 10.1016/j.actamat.2014.10.002.

[3] L., X. A unified expression for low cycle fatigue and extremely low cycle fatigue and its implication for monotonic loading. *International Journal of Fatigue*, 30:1691–1698 (2008). doi:10.1016/j.ijfatigue.2008.03.004.

[4] Kuroda, M. Extremely low cycle fatigue life prediction based on a new cumulative fatigue damage model. *International Journal of Fatigue*, 24(6):699–703 (2002).

[5] Pereira, J. C. R., de Jesus, A. M. P., Xavier, J., and Fernandes, A. A. Ultra low-cycle fatigue behaviour of a structural steel. *Engineering Structures*, 60:214–222 (2014).

[6] Park, Y. S., J., P. S., Iwai, S., and Kang, S. H. Failure and damage of steel thin-plate elements and angle members due to very-low-cycle loading. *Engineering Structures*, 26:1623–1632 (2004).

[7] Halama, R. Experimentální poznatky a fenomenologické modelování cyklické plasticity kovů. *Habilitační práce, VŠB – Technická univerzita Ostrava, Fakulta strojní* (2009).

[8] *ABAQUS/Standard User's Manual, Version 6.14*. Dassault Systèmes Simulia Corp, United States (2014).

[9] Chaboche, J. L., Dang, V. K., and Cordier, G. Modelization of the Strain Memory Effect on the Cyclic Hardening of 316 Stainless Steel. *Proceedings of the 5th International Conference on Structural Mechanics in Reactor Technology, Berlin*, pages 1–10 (1979).

[10] Marquis, D. Modélisation et identification de l'écrouissage anisotrope des métaux. *Thése de 3éme cycle, Université Paris 6, France.* (1979).

[11] Halama, R., Sedlák, J., and Šofer. M. Phenomenological Modelling of Cyclic Plasticity. *Numerical Modelling Miidla, Miidla, P., Ed.; IntechOpen: London, UK*, pages 329–354 (2012).

[12] Kopas, P., Saga, M., Baniari, V., Vasko, M., and Handrik, M. A plastic strain and stress analysis of bending and torsion fatigue specimens in the low-cycle fatigue region using the finite element methods. *Procedia Engineering*, 177:526–531 (2017).

[13] Chen, X., Chen, X., Yu, D., and Gao, B. Recent progresses in experimental investigation and finite element analysis of ratcheting in pressurized piping. *International Journal of Pressure Vessels and Piping*, 101:113–142 (2013). doi:https://doi.org/10.1016/j.ijpvp.2012.10.008.

[14] Armstrong, P. J. and Frederick, C. O. A Mathematical Representation of the Multiaxial Bauschinger Effect. *G.E.G.B. Report RD/B/N*, 731 (1966).

[15] Ohno, N. and Wang, J. D. Kinematic Hardening Rules with Critical State of Dynamic Recovery. Part I: Formulation and Basic Features for Ratchetting Behavior. *International Journal of Plasticity*, 9:375–390 (1993).

[16] Abdel-Karim, M. and Ohno, N. Kinematic hardening model suitable for ratchetting with steady-state. *Internation Journal of Plasticity*, 16:225–240 (2000).

[17] Halama, R., Fusek, M., Šofer, M., Poruba, Z., Matušek, P., and Fajkoš, R. Ratcheting Behavior of Class C Wheel Steel and Its Prediction by Modified AbdelKarim-Ohno Model. In *roceedings of the 10th International Conference on Contact Mechanics CM2015*. Colorado Springs, Colorado, USA (2015).

[18] Feigenbaum, H. P. and Dafalias, Y. F. Directional distortional hardening in metal plasticity within thermodynamics. *International Journal of Solids and Structures*, 44:7526–7542 (2007).

[19] Parma, S., Plešek, J., Marek, R., Hrubý, Z., Feigenbaum, H. P., and Dafalias, Y. F. Calibration of a simple directional distortional hardening model for metal plasticity. *International Journal of Solids and Structures*, 143:113–124 (2018).

[20] Sung, S. J., Liu, L. W., Hong, H. K., and Wu, H. C. Evolution of yield surface in the 2D and 3D stress spaces. *International Journal of Solids and Structures*, 48:1054–1069 (2011).

[21] Ohno, N. A constitutive model of cyclic plasticity with a nonhardening strain region. *Journal of Applied Mechanics*, 49:721–727 (1982).

[22] Jiang, Y. and Sehitoglu, H. Modeling of cyclic ratchetting plasticity, part I: Development of constitutive relations. *Journal of Applied Mechanics*, 63:720–725 (1996).

[23] Kang, G. Z., Ohno, N., and Nebu, A. Constitutive modeling of strain-range dependent cyclic hardening. *International Journal of Plasticity*, 19:1801–1819 (2003).

[24] Metallic materials - Tensile testing - Part 1: Method of test at room temperature. Standard, International Organization for Standardization, CH-1214 Vernier, Geneva, Switzerland (2016).

[25] Chaboche, J. L. and Lemaitre, J. *Mechanics of Solid Materials*. Cambridge University Press, Cambridge (1990).

[26] Standard Practise for Strain-Controlled Fatigue Testing. Standard, ASTM International, West Conshohocken, PA, USA (1998).

Publications and Other Achievements of the Author Related to Topic of the Thesis

Published Papers

[A1] Halama, R., Fumfera, J., Gál, P., Kumar, T., Markopoulos, A. Modeling the Strain-Range Dependent Cyclic Hardening of SS304 and 08Ch18N10T Stainless Steel with a Memory Surface. *Metals*, 9(832):1-26 (2019).

[A2] Fumfera, J., Halama, R., Procházka, R., Gál, P., Španiel, M. Strain Range Dependent Cyclic Hardening of 08Ch18N10T Stainless Steel—Experiments and Simulations. *Materials*, 12(4243):1-28 (2019).

Conference Contributions

[A3] Fumfera, J., Halama, R., Kuželka, J., Španiel, M. Strain-Range Dependent Cyclic Plasticity Material Model Calibration for the 08Ch18N10T Steel. In: *Proceedings of the 33rd conference with international participation on Computational Mechanics 2017*. Pilsen: University of West Bohemia, p. 25-26, (2017). ISBN 978-80-261-0748-4.

[A4] Fumfera, J., Džugan, J., Kuželka, J., Procházka, R., Španiel, M. Strain-amplitude Dependent Cyclic Hardening of 08Ch18N10T Austenitic Stainless Steel. In: *4th International Conference Recent Trends in Structural Materials, COMAT 2016*. London: Institute of Physics Publishing, IOP Conference Series: Materials Science and Engineering. vol. 179 (2017). ISSN 1757-8981.

[A5] Fumfera, J., Procházka, R. Specimen design for low-cycle fatigue experiments under large strain amplitude loading. In: *Experimental Stress Analysis 2016*. Plzeň: Západočeská universita, Fakulta aplikovaných věd, (2016). ISBN 978-80-261-0624-1.

Research Reports

[A6] Fumfera, J., Kuželka, J., Španiel, M. *Simulace zatížení příruby*. 12105/17/35. [Research report]. Prague: Czech Technical University in Prague, Faculty of Mechanical Engineering, (2017). [in Czech].

[A7] Fumfera, J., Kuželka, J., Španiel, M. *Popis programového skriptu pro identifikaci parametrů Halamova modelu cyklické plasticity*.

12105/17/34. [Research report]. Prague: Czech Technical University in Prague, Faculty of Mechanical Engineering, (2017). [in Czech].

[A8] Fumfera, J., Kuželka, J., Španiel, M. *Určení deformace vzorků.* 12105/17/11. [Research report]. Prague: Czech Technical University in Prague, Faculty of Mechanical Engineering, (2017). [in Czech].

[A9] Fumfera, J., Kuželka, J., Španiel, M. *Materiálový model cyklické plasticity s cyklickým zpevněním závislým na hladině zatížení a jeho kalibrace.* 12105/17/10. [Research report]. Prague: Czech Technical University in Prague, Faculty of Mechanical Engineering, (2017). [in Czech].

[A10] Fumfera, J. *Návrh parametrů zatěžování pro vrubované vzorky.* 12105/15/17. [Research report]. Prague: Czech Technical University in Prague, Faculty of Mechanical Engineering, (2015). [in Czech].

[A11] Fumfera, J. *Návrh vzorků a parametrů zatěžování.* 12105/15/02. [Research report]. Prague: Czech Technical University in Prague, Faculty of Mechanical Engineering, (2015). [in Czech].

Software

[A12] Kuželka, J., Fumfera, J., Džugan, J., Petruška, J., Lopaur, J., Hůlka, J. Plugin pro hodnocení a identifikaci cyklické plasticity kovových materiálů. [Software]. (2015).